An effective and efficient model of the near-field hydrodynamic interactions for active suspensions of bacteria

Bokai Zhang[a,b], Premkumar Leishangthem[a], Yang Ding (丁阳)[c,d,1], and Xinliang Xu[a,d,1]

[a]Complex Systems Division, Beijing Computational Science Research Center, Beijing 100193, China; [b]Department of Physics, Zhejiang Sci-Tech University, Hangzhou 310018, China; [c]Mechanics Division, Beijing Computational Science Research Center, Beijing 100193, China; and [d]Department of Physics, Beijing Normal University, Beijing 100875, China

Edited by David A. Weitz, Harvard University, Cambridge, MA, and approved June 1, 2021 (received for review January 5, 2021)

Near-field hydrodynamic interactions in active fluids are essential to determine many important emergent behaviors observed, but have not been successfully modeled so far. In this work, we propose an effective model capturing the essence of the near-field hydrodynamic interactions through a tensorial coefficient of resistance, validated numerically by a pedagogic model system consisting of an *Escherichia coli* bacterium and a passive sphere. In a critical test case that studies the scattering angle of the bacterium–sphere pair dynamics, we prove that the near-field hydrodynamics can make a qualitative difference even for this simple two-body system: Calculations based on the proposed model reveal a region in parameter space where the bacterium is trapped by the passive sphere, a phenomenon that is regularly observed in experiments but cannot be explained by any existing model. In the end, we demonstrate that our model also leads to efficient simulation of active fluids with tens of thousands of bacteria, sufficiently large for investigations of many emergent behaviors.

bacterial motion | near-field hydrodynamics | low Reynolds number fluid

Dense suspensions of microorganisms swimming in complex environments are ubiquitous in nature. The hydrodynamic interactions (HI) among many thousands of microorganisms and the surrounding boundary give rise to novel emergent behaviors at macroscopic length scales, for example, self-organization (1–3), active turbulence (4, 5), and bacterial "superfluid" (6, 7). Such behaviors not only are important for fundamental bioprocesses [e.g., fluid transport in bacterial colonies (8)] but also have practical implications [e.g., design of microfluidic structures (9) and artificial microswimmers (10, 11) for desired transport properties]. To understand these large-scale behaviors in active suspensions, it is essential to have a simple model that is able to describe the near-field HI with both physical effectiveness and computational efficiency, as negligence of near-field HI is known to lead to erroneous system dynamical behaviors and structures (12, 13), and accurate description of the near-field HI by direct numerical calculations is limited to few-body systems, due to computational complexity (14, 15). However, despite its fundamental importance, development of such a model of near-field HI has been a long-standing problem, and is the subject of this work.

For a system of only a few microorganisms, the HI can be evaluated numerically at arbitrary accuracy by brute force [e.g., the method of Stokeslets (14) or boundary element method (15)]. From these studies, it is demonstrated that, by treating an *Escherichia coli* bacterium as an assembly of one head and helical flagella with no-slip boundary (Fig. 1*A*), HI in the near-field limit is essential for bacterial dynamical behaviors (16). However, for large suspensions with tens of thousands of microorganisms, the computational complexity to accurately describe the HI for swimmers (micrometers in size) at near-touching scenario (surface distance around 10 nm) makes such brute force approaches infeasible in the foreseeable future. A simple model of the HI, which provides explicit functional form for any given swimmer configurations, is needed.

At this point, it is worthwhile to point out that a model of microoganisms (which describes the intrinsic surface properties of a microorganism, e.g., squirmer model of a rigid spherical cell with prescribed surface velocity that mimics spherical ciliates) should not be mistaken for our focus here of a model of HI (which generalizes the behavior of the stress distribution on the surface of the microorganism as a function of configuration). One good example of the latter is the dipole model, which treats the stress distribution of one bacterium as a force dipole (17, 18). This simple model is successful in predicting the enhanced diffusion of tracer particles (19, 20), but is only accurate for the far field and requires a cutoff size to avoid the unphysical divergence at the location of the force dipole.

For *E. coli* bacteria, a more realistic model treats each bacterium as two beads connected by a rigid rod, and models the stress distribution as two point forces located at the centers of these two beads that are separated by a length of l (Fig. 1*B*). In this two-bead model, the tail bead is propelled by a force $\boldsymbol{F}_{act}$, provided by flagella that are not treated explicitly. Then, according to the force balance on each bead, the forces exerted on fluid are simply $\boldsymbol{F}_{eff}$ and $-\boldsymbol{F}_{eff}$ for the head and tail beads, respectively.

Significance

Active suspensions of microswimmers demonstrate novel emergent behaviors (self-organizations, active turbulence, etc.) on macroscopic length scales. For such systems with, minimally, thousands of microswimmers, direct numerical simulations of the hydrodynamic interactions are computationally infeasible, and reduced models are needed. We demonstrated that existing models are not satisfactory in describing the hydrodynamic interactions for microswimmers in close proximity with even qualitatively erroneous predictions, indicating a pressing need for an adequate model. We propose a model that is both physically effective and computationally efficient in describing such hydrodynamics. The main novelty of our model is the description of hydrodynamic interactions through a resistance tensor, as opposed to an effective steric interaction in existing models.

Author contributions: Y.D. and X.X. designed research; B.Z., P.L., Y.D., and X.X. performed research; B.Z., P.L., and X.X. analyzed data; and Y.D. and X.X. wrote the paper.

The authors declare no competing interest.

This article is a PNAS Direct Submission.

[1]To whom correspondence may be addressed. Email: dingyang@csrc.ac.cn or xinliang@csrc.ac.cn.

This article contains supporting information online at https://www.pnas.org/lookup/suppl/doi:10.1073/pnas.2100145118/-/DCSupplemental.

Published July 6, 2021.

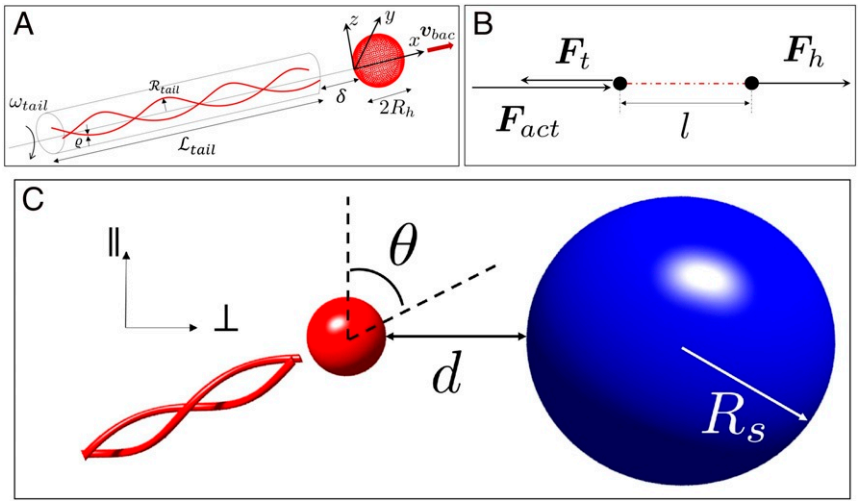

Fig. 1. The system at study. (*A*) Our model *E. coli*. (*B*) The bacterial stress distribution is described as two point forces ($\boldsymbol{F}_h = \boldsymbol{F}_{eff}$ for the head and $\boldsymbol{F}_t = -\boldsymbol{F}_{eff}$ for the tails) separated by *l*. The propulsive force arising from the spinning of the tails is $\boldsymbol{F}_{act}$. (*C*) Our pedagogic system of one bacterium (red) and one passive sphere (blue).

Models of this type have been applied for both pushers and pullers (21) in various studies, including bacterial motion near a plane wall (22), two hydrodynamically interacting bacteria (23, 24), and the collective motions in a suspension (25). However, in the near-field limit, the stress distributions on bacterial surfaces change so dramatically that the use of two fixed point forces becomes an oversimplification incapable of capturing the essence of the HI. Insisting on the use of such an oversimplification brings severe unphysical consequences, for example, invariant $\boldsymbol{F}_{eff}$ with respect to a nonactive bacterium and invariant $\boldsymbol{v}_{bac}$ (bacterial self-swimming velocity) independent of the surrounding environment (21, 25), which inevitably leads to artificial overlaps between bacteria. To solve the catastrophic overlap problem shared by this type of model, one brute-force approach commonly used is to introduce a repulsive steric interaction. But the use of an effective repulsion in place of the near-field hydrodynamics leads to erroneous predictions in both individual swimming motion (such as incorrect estimate of $\boldsymbol{F}_{eff}$ and unrealistically fast separation for bacterial pairs in close proximity) and macroscopic structures [such as clustering (13)].

The near-field HI between two microorganisms has also been modeled for eukaryotes that are simplified as squirmers (26). Yet the study is severely limited due to the use of ideal assumptions of spherical shape and a prescribed surface velocity that is configuration independent (27). While the former assumption makes the squirmer unable to respond to the local strain of the external flow, the latter assumption is qualitatively inconsistent with experimental observations (28) and leads to unphysical work output that diverges at zero surface distance (26).

In this work, we examine the key ingredients of the existing two-bead model upon which we can build our model, as well as the defects of the existing two-bead model that need to be corrected. Since the characteristic size and speed of most bacteria are about 1 μm and 10 μm/s, respectively, in water, the corresponding Reynolds number is very low (10^{-5} to 10^{-2}). Therefore, bacterial flows are typically studied approximately by the linear Stokes equation. By exploiting the linearity of the governing Stokes equation, the many-body HI problem can be reduced to the pedagogic problem of the HI between one passive sphere and one bacterium (26, 29). Specifically, the pedagogic system presented in this study consists of one free passive sphere with radius R_s, and an *E. coli*–shaped bacterium with fixed bacterial motor rotation rate ω_0 (30), both immersed in a fluid of viscosity μ (Fig. 1*C*). The bacterium is modeled as an assembly of a spherical head of diameter σ defined as the unit length, and two helical flagella, with a gap δ in between for computational stability. The HI are then quantitatively evaluated by solving the linear Stokes equation with no-slip boundary conditions on the surfaces of the passive sphere and the bacterium, at configurations defined by the surface distance d, incoming angle θ (negative θ corresponds to the "nose down" situation with bacterium moving toward the passive sphere), and R_s, as illustrated in Fig. 1*C*. The Stokes equation with moving boundaries can be routinely solved using the numerical method of Stokeslets (14, 31), where the boundary surfaces are divided into a large number of small regions, and the stress distributed on each region is then approximated by a point force. This method is based on the fact that the creeping flow $\boldsymbol{u}$ at location $\boldsymbol{r}'$ due to each point force $\boldsymbol{f}$ at location $\boldsymbol{r}_0$ is analytically available as

$$\boldsymbol{u}(\boldsymbol{r}') = \boldsymbol{G}(\boldsymbol{r}', \boldsymbol{r}_0)\boldsymbol{F}(\boldsymbol{r}_0), \qquad [1]$$

where $\boldsymbol{G}$ is a fundamental solution to the linear Stokes equation and is called a Stokeslet. The Stokeslet in three dimensions manifests in the tensor form of $G_{ij}(\boldsymbol{r}', \boldsymbol{r}_0) = (1/8\pi\mu)(\delta_{ij}/r + r_i r_j / r^3)$, with $r \equiv |\boldsymbol{r}| \equiv |\boldsymbol{r}' - \boldsymbol{r}_0|$. Then the solution of the entire flow field is the sum of all of the flows, each generated by one of these point forces.

The dependence of instantaneous speed of the passive sphere, $|\boldsymbol{v}_s|$, on the surface distance d at a few typical incoming angles θ and sphere radii R_s is shown in Fig. 2*A*. At large d, $|\boldsymbol{v}_s|$ always decays as d^{-2}, regardless of θ and R_s. This power-law decay is consistent with previous experimental observations (18) as well as the predictions of the dipole model (19). At intermediate d, $|\boldsymbol{v}_s|$ behaves qualitatively differently from the dipole predictions; for example, at $R_s = 50$, a nonmonotonic behavior of $|\boldsymbol{v}_s|$ is observed.

To explain $|\boldsymbol{v}_s|$ at intermediate d, we follow the existing two-bead model by treating the bacterium as two point forces. To do so, we add all of the point forces on bacterium head (tail) as obtained in Stokeslets method and place the sum $\boldsymbol{F}_{eff} = \sum_{n=1}^{N_{head}} \boldsymbol{F}_n$ ($-\boldsymbol{F}_{eff}$ for the tail as dictated by the force-free condition) at $\boldsymbol{r}_h$ ($\boldsymbol{r}_t$), the geometric center of the head (tail). Induced by these two point forces that are separated by l (Fig. 1*B*), the motion of the passive sphere follows Faxen's law,

$$\boldsymbol{v}_s = \left(1 + \frac{R_s^2}{6}\nabla^2\right)\boldsymbol{u}(\boldsymbol{r})\Big|_{\boldsymbol{r}=\boldsymbol{r}_0}, \qquad [2]$$

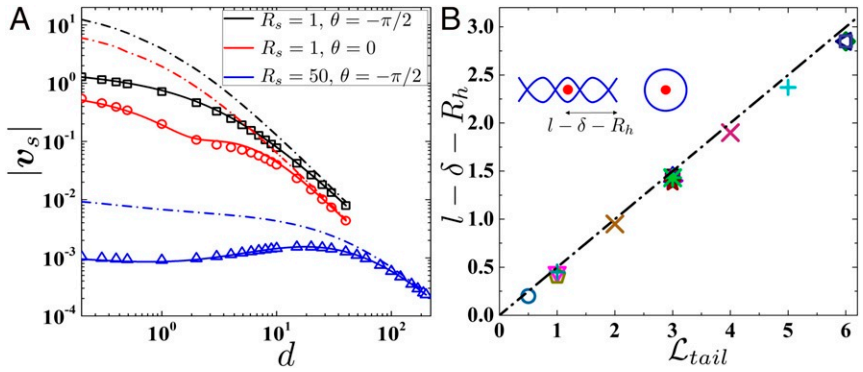

Fig. 2. (*A*) The $|\boldsymbol{v}_s|$ as a function of d for a few typical θ and R_s, obtained from the method of Stokeslets (symbols), the dipole model (dash-dotted lines), and the two-bead model (solid lines). (*B*) The location of the point force that models the tail, obtained through a fit of our numerical results. The two red dots in the *Inset* illustrate the locations of the two point forces. Different symbols and colors in *B* represent different species in *SI Appendix*, Table S1. The dash-dotted line indicates location of the geometric center of the tails.

where $\boldsymbol{r}_0$ is the location of the spherical center, and $\boldsymbol{u}(\boldsymbol{r})$ is the flow generated by the two point forces. Using $\boldsymbol{F}_{eff}$ and the fixed locations of the point forces as input, the predictions of $\boldsymbol{v}_s$ obtained from Eq. **2** agree very well with our numerically obtained results from the Stokeslets method at both large and intermediate d (Fig. 2*A*). The nonmonotonic behavior observed for large passive sphere cases is due to the competition between R_s and the characteristic length of the flow gradient dictated by l.

The above quantitative agreement regarding $\boldsymbol{v}_s$ supports a key ingredient of the existing two-bead model that treats the locations of the two point forces as bacterial intrinsic properties. The validity of this treatment can be further demonstrated, using bacteria of different tail shapes characterized by the following parameters: helical length L_{tail}, helical radius R_{tail}, and number of helical pitches N_p (specific choices of these parameters are available in *SI Appendix*, Table S1). For each specific bacterial shape, using the method of Stokeslets, we again compute the stress distribution $\boldsymbol{f}_n$ on the bacterial surface and the motion of the passive sphere $\boldsymbol{v}_s$ at many different configurations defined by d, θ, and R_s. For each configuration, we again place $\boldsymbol{F}_{eff} = \sum_{n=1}^{N_{head}} \boldsymbol{F}_n$ at $\boldsymbol{r}_h$, the geometric center of the head, and place $-\boldsymbol{F}_{eff}$ at a location on the longitudinal axis that is l away from $\boldsymbol{r}_h$ (Fig. 2*B*, *Inset*). Then, according to Eq. **2**, l can be treated as a free parameter and obtained through a fit of numerically obtained $\boldsymbol{v}_s$ at all configurations. The fitting result for each specific bacterial shape is illustrated in Fig. 2*B*, where the location of the $-\boldsymbol{F}_{eff}$ for each bacterium shape is very close to $\boldsymbol{r}_t$, the geometric center of the tails (dash-dotted line in Fig. 2*B*), supporting our argument that the locations of the two point forces are bacterial intrinsic properties.

However, unlike the predictions of the existing two-bead model (21, 25) that bacterial motion $\boldsymbol{v}_{bac}$ and the force $\boldsymbol{F}_{eff}$ are both invariant when the bacterium is swimming among passive objects, our numerical results show otherwise. This qualitative difference can be best illustrated as in Fig. 3*A*, where we show $|\boldsymbol{v}_{bac}|$ and $|\boldsymbol{F}_{eff}|$ (Fig. 3*A*, *Inset*) as functions of d, at $\theta = -\pi/2$ (the bacterium moving toward the center of the passive sphere) for two typical sphere radii $R_s = 1$ and $R_s = 100$, respectively. For $d \gg 1$, the influence of the passive sphere on the bacterium is negligible, so that $|\boldsymbol{v}_{bac}|$ and $|\boldsymbol{F}_{eff}|$ reduce to their correspondence for a solitary bacterium: v^0_{bac} and F^0_{eff}, respectively. At smaller d, we see a significant decrease in bacterium swimming velocity, from v^0_{bac} to $|\boldsymbol{v}_{bac}|(d = 0.1) \approx 0.3 v^0_{bac}$ in the system with $R_s = 100$, presumably due to the increase of effective resistance felt by the bacterium. In the same small d regime, we see that $|\boldsymbol{F}_{eff}|$ increases noticeably from F^0_{eff}.

We propose that the key to the observed strong dependence of $\boldsymbol{v}_{bac}$ and $\boldsymbol{F}_{eff}$ on surface distance d is the near-field HI between the bacterium and the sphere, which can be quantitatively modeled by the resistance tensor $\boldsymbol{\xi}$, defined as in

$$\begin{pmatrix} \boldsymbol{F}_h \\ \boldsymbol{F}_s \\ \boldsymbol{F}_t \\ \boldsymbol{T}_h \end{pmatrix} = \boldsymbol{\xi} \cdot \begin{pmatrix} \boldsymbol{v}_h \\ \boldsymbol{v}_s \\ \boldsymbol{v}_t - \boldsymbol{v}_0 \\ \boldsymbol{\Omega}_{bac} \end{pmatrix} \text{ with } \boldsymbol{\xi} = \begin{pmatrix} \boldsymbol{\xi}_{hh} & \boldsymbol{\xi}_{hs} & \boldsymbol{\xi}_{ht} & \boldsymbol{0} \\ \boldsymbol{\xi}_{sh} & \boldsymbol{\xi}_{ss} & \boldsymbol{\xi}_{st} & \boldsymbol{0} \\ \boldsymbol{\xi}_{th} & \boldsymbol{\xi}_{ts} & \boldsymbol{\xi}_{tt} & \boldsymbol{0} \\ \boldsymbol{\xi}^{TU}_{hh} & \boldsymbol{\xi}^{TU}_{hs} & \boldsymbol{0} & \boldsymbol{\xi}^{T\Omega}_{hh} \end{pmatrix}, \quad [3]$$

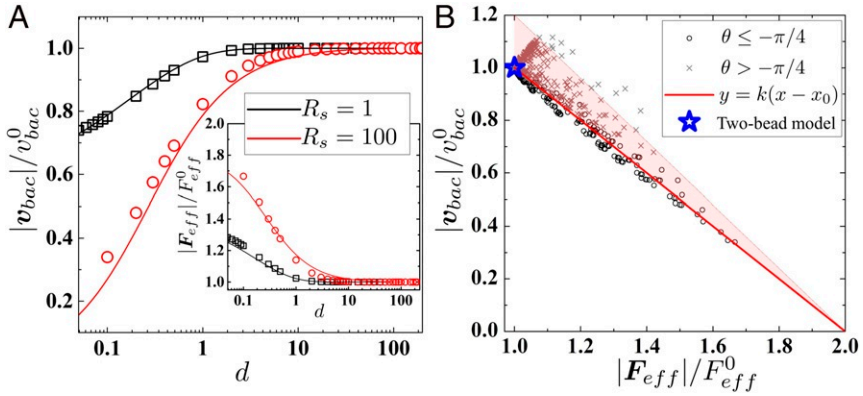

Fig. 3. Configuration-dependent $\boldsymbol{v}_{bac}$ and $\boldsymbol{F}_{eff}$. (*A*) Our model predictions based on Eq. **3** (solid lines) and numerical results from the method of Stokeslets (symbols) for $|\boldsymbol{v}_{bac}|$ and $|\boldsymbol{F}_{eff}|$ (*Inset*), with $R_s = 1$ (black) and $R_s = 100$ (red). (*B*) All numerical data obtained from the method of Stokeslets (symbols) collapse onto a master curve as predicted by Eq. **4** (solid line). Shaded area represents $k(x - x_0) < y < 1.2 \times k(x - x_0)$. The existing two-bead model predicts that all data would collapse to a single point (blue star).

where $\boldsymbol{F}_h = \boldsymbol{F}_{eff}$, $\boldsymbol{F}_t = -\boldsymbol{F}_{eff}$, and $\boldsymbol{F}_s = 0$ are the forces exerted by the bacterial head, tails, and the passive sphere, respectively; $\boldsymbol{T}_h \equiv \boldsymbol{F}_{eff} \times (\boldsymbol{r}_h - \boldsymbol{r}_t)$ is the torque exerted by bacterial head; $\boldsymbol{v}_h$, $\boldsymbol{v}_t$, and $\boldsymbol{v}_s$ are the velocities of the bacterial head, tails, and passive sphere, respectively; $\boldsymbol{\Omega}_{bac} \equiv (\boldsymbol{r}_h - \boldsymbol{r}_t) \times (\boldsymbol{v}_h - \boldsymbol{v}_t)/l^2$ is the bacterial rotation around its center of mass; and $\boldsymbol{v}_0 \equiv \boldsymbol{\xi}_{tt}^{-1} \cdot \boldsymbol{F}_{act}$ (see *SI Appendix* for details of derivation). The last row of Eq. **3**, $\boldsymbol{\xi}_{hh}^{TU} \cdot \boldsymbol{v}_h + \boldsymbol{\xi}_{hs}^{TU} \cdot \boldsymbol{v}_s + \boldsymbol{\xi}_{hh}^{T\Omega} \cdot \boldsymbol{\Omega}_{bac} = \boldsymbol{F}_{eff} \times (\boldsymbol{r}_h - \boldsymbol{r}_t)$, is just the torque balance condition previously derived (32), which is trivial for the one-dimensional problem (e.g., the bacterium moving toward the center of the passive sphere) but becomes nontrivial when the rotational motion is strong.

Since the tail flagella are very thin (~ 10 nm) compared to the head (~ 1 μm), in the simplest consideration, we can assume that the tails are not as affected by the near-field HI. That is, the force $\boldsymbol{F}_{act}$ arising from the spinning of the tails around the longitudinal direction is configuration independent, and the terms in $\boldsymbol{\xi}$ involving the tails retain their far-field values. Then the near-field HI only appears in tensor elements $\boldsymbol{\xi}_{hh}$, $\boldsymbol{\xi}_{hs}$, $\boldsymbol{\xi}_{ss}$, $\boldsymbol{\xi}_{hh}^{TU}$, $\boldsymbol{\xi}_{hs}^{TU}$, and $\boldsymbol{\xi}_{hh}^{T\Omega}$, and we can solve $\boldsymbol{F}_{eff}$ and $\boldsymbol{v}_{bac}$ as functions of $\boldsymbol{F}_{act}$ and $\boldsymbol{\xi}$. In the $d \to 0$ limit, lubrication theory shows that these relevant tensor elements can all be written as analytic functions of only one parameter, the nondimensional surface distance $2d/(0.5 + R_s)$ (33). To keep our model simple, at finite d, we write these tensor elements by extrapolating the analytical lubrication forms regarding the single parameter $2d/(0.5 + R_s)$. Thus, using $\boldsymbol{F}_{act}$, $\boldsymbol{\xi}$, and the fixed locations of the two point forces as input, we can solve Eq. **3** for $\boldsymbol{F}_{eff}$ and $\boldsymbol{v}_{bac}$.

As illustrated in Fig. 3*A*, our model captures the near-field HI by reproducing the slowing down of the bacterium as it closes in the passive sphere at $\theta = -\pi/2$, for two typical radii, $R_s = 1$ and $R_s = 100$. Specifically, our model predictions for both $\boldsymbol{F}_{eff}$ and $\boldsymbol{v}_{bac}$ show a quantitative agreement with numerical results from Stokeslets method at all ranges of d. More importantly, our model naturally amended the disastrous overlap problem in the existing two-bead model: In the limit of $d \to 0$, the terms in the resistance tensor that correspond to the relative motion between the bacterial head and the passive sphere diverge, leading to an infinitesimal relative motion (33).

Below, we test whether the proposed idea of modeling the near-field HI entirely through the resistance tensor can be applied to more general systems where an analytical form may not be available. Using, again, the approximation that tail flagella are thin (so that $\boldsymbol{F}_{act}$ is a constant, and terms in $\boldsymbol{\xi}_{tt}$ are constants and much larger than terms in $\boldsymbol{\xi}_{st}$), it can be shown that Eq. **3** leads to a generic linear relation between $\boldsymbol{F}_{eff}$ and $\boldsymbol{v}_{bac}$ regardless of the shapes of the bacterial head and the passive object (see *SI Appendix* for derivation):

$$\frac{|\boldsymbol{v}_{bac}|}{v_{bac}^0} = k \times \left(\frac{|\boldsymbol{F}_{eff}|}{F_{eff}^0} - x_0 \right), \qquad [4]$$

where the slope $k = (F_{eff}^0/F_{eff}^0 - F_{act})$ and intercept $x_0 = F_{act}/F_{eff}^0$ are both bacterial intrinsic properties. As illustrated in Fig. 3*B*, this generic linear relation is strongly supported by the collapse of all data obtained through the method of Stokeslets onto the predicted straight line, in comparison to the predicted collapse onto a single point $|\boldsymbol{v}_{bac}|/v_{bac}^0 = |\boldsymbol{F}_{eff}|/F_{eff}^0 = 1$ by the existing two-bead model. While our calculations show that the simplified treatment of $\boldsymbol{F}_{act}$ as a constant is responsible for the deviations between the predicted straight line and our numerical data, these deviations are small, supporting our argument that the change in $\boldsymbol{F}_{act}$ is not essential for our simple model. The qualitative agreement between our predicted linear relation and numerical data shows that a qualitative description of the resistance tensor can be sufficient in capturing the essence of the near-field HI, and therefore applies to more general systems with bacterial head of arbitrary shapes.

In the following, we show that our effective model of the near-field HI is essential in obtaining the correct bacterial dynamic behavior through an investigation of the scattering angle out of the bacterium–sphere pair dynamics. Considering a free passive sphere at the origin and a bacterium at $x = -\infty$ and $y = b$ moving toward the $+x$ direction, we studied the dependence of the scattering angle ψ on impact parameter b/R_s and bacterium–sphere size ratio l/R_s (Fig. 4*A*). Our model predicts that there exists a critical size for the passive sphere in the presence of near-field HI. For spheres larger than this critical size, the bacterium can be entrapped by the passive sphere with an orbital motion (Fig. 4*B*), which can be related to a stable fixed point in the two-dimensional phase plane defined by d and θ (Fig. 4*D*). This entrapment of bacterium is also obtained numerically using the method of Stokeslets (*SI Appendix*, Fig. S2), and has been regularly observed in experiments (32, 34). Contrarily, no such entrapment can be reproduced by existing models that use a repulsive steric interaction in place of our tensorial description of the near-field HI, regardless of the specific form chosen for the steric repulsion (Fig. 4 *C* and *F*). The numerical results above show that the resistance tensor captures the essence of the near-field HI and cannot be replaced by any effective steric interactions. A previous model has also studied the entrapment numerically (35), by simplifying the bacterial stress distribution as a force dipole and evaluating its near-field HI with the passive sphere through the method of images. However, as the surface distance d becomes very small during the entrapment, the dipole approximation becomes an oversimplification insufficient to describe the stress distributions, since higher-order terms in the multipole expansion are also very important (36). Therefore, unlike our model that predicts a stable fixed point, calculations based on this previous model show only one saddle point in the phase plane (the red cross in Fig. 4*E*). And the seeming entrapment observed in this previous work is merely the unphysical consequence of an artificially imposed condition of a minimum surface distance (the black circle in Fig. 4*E*).

Beyond being physically effective, our model of the near-field HI through the resistance tensor also leads to efficient simulation of large bacterial suspensions. To construct such a resistance tensor, we follow the classic Stokesian dynamics simulation (29), which reduces the many-body HI problem to a two-body HI problem in a two-step procedure by exploiting the linearity of the Stokes equation. Specifically, in the first step, we model the HI at far-field limit through the grand mobility tensor $\boldsymbol{M}_0$, which can be analytically constructed in a pairwise addictive fashion by assuming simply a point force at the center of each bead. In the second step, the resistance tensor is obtained, as analytical lubrication terms for near-touching pairs, $\boldsymbol{\xi}_{2b}$, are included in a pairwise additive fashion: $\boldsymbol{\xi} = \boldsymbol{M}_0^{-1} + \boldsymbol{\xi}_{2b}$. In our simulation, we implement the solution of the linear equation $\boldsymbol{\xi} \cdot \boldsymbol{v} = \boldsymbol{F}$ by first transforming it into an equivalent form of $(\boldsymbol{I} + \boldsymbol{M}_0 \cdot \boldsymbol{\xi}_{2b}) \cdot \boldsymbol{v} = \boldsymbol{M}_0 \cdot \boldsymbol{F}$ and then solving it with General Minimal Residual Method (GMRES). As illustrated in Fig. 5*A*, our model enables efficient simulations of active suspensions with N swimmers by evaluating HI in 10 to 100 s, where N = 1,000 for a laptop (Intel i5, 8-GB memory), N = 3,000 for a desktop (Intel i9-9820X, 64-GB memory), and N = 10,000 for a single computational node (two Intel Xeon E5-2680 v3 chips, 256-GB memory). These numbers are sufficiently large to investigate the essential influence of near-field HI on many emergent behaviors displayed in active fluids, as illustrated by previous studies with models that are unable to capture the near-field HI [e.g., N = 2,500 in studying hydrodynamic instability (5), N = 1,000 in studying the effect of confinement (25), and $N = 200$ in

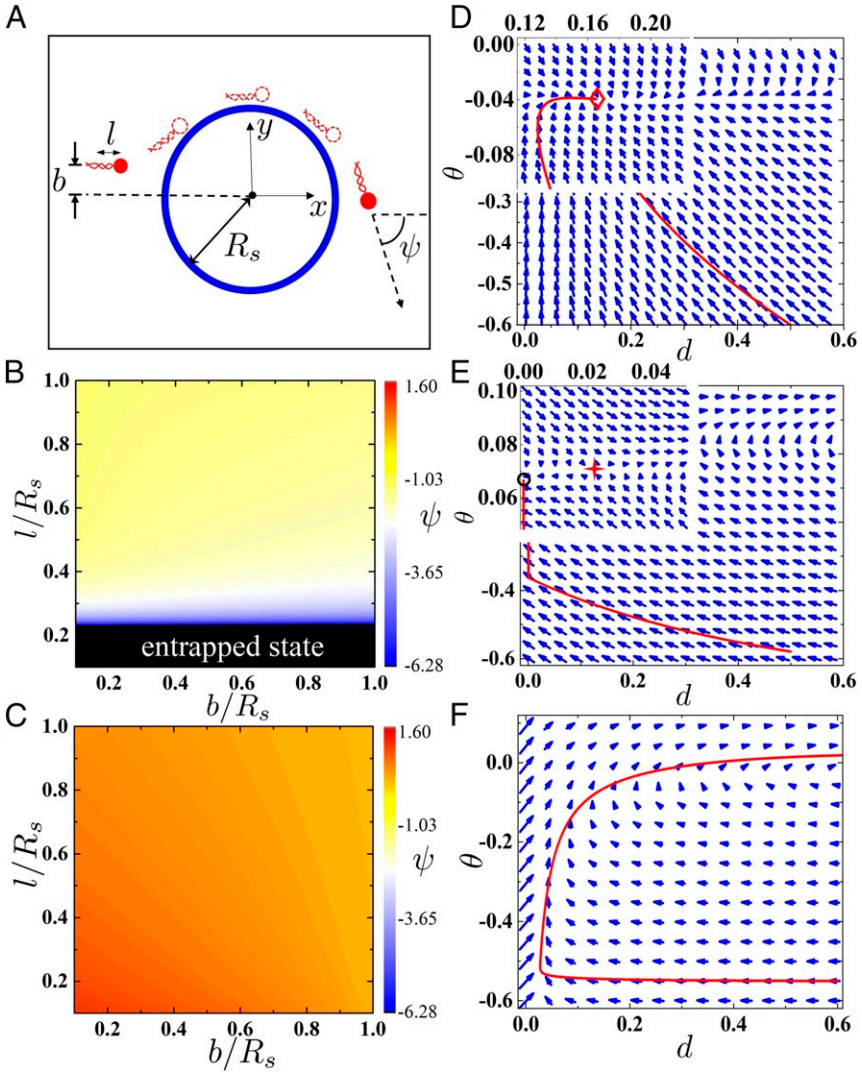

Fig. 4. Bacterial entrapment. (*A*) Setup for the scattering problem, where ψ is positive for counterclockwise rotation. Contour map of ψ is predicted by (*B*) our model and (*C*) the existing two-bead model. The trajectory of a bacterium (red line) in the phase plane defined by d and θ as predicted by (*D*) our model, (*E*) an earlier study using image of a force dipole, and (*F*) the existing two-bead model. A closer look at the trajectory in *D* shows a stable fixed point (red square). In *E*, there only exists a saddle point (red cross), and the entrapment is artificially obtained with a sticky steric interaction at $d = 0$ (black circle).

studying the emergence of organizations (1)]. A snapshot of the flow field out of our simulation with $N = 1{,}000$ is illustrated (Fig. 5*B*), which reproduces the vortex structures that have been observed in earlier simulation works (25). It is worthwhile to note that, without a simple model, an accurate description the near-field HI for even a small system of $N = 10$ through the method of Stokeslets requires days of computation. Direct numerical simulations [e.g., the multiparticle collision dynamics (37, 38), the lattice Boltzmann method (39), or the smooth profile method (40)] alternatively evaluate the HI by explicit calculation of solvent motion. However, to resolve the near-field HI requires advanced techniques such as grid refinement, which leads to expensive computations, as the simulation time step scales linearly with the smallest grid size. Even by employing a steric repulsion that avoids proper treatment of HI in the near-field limit, these direct numerical simulations are typically used for small system of $N \approx 100$.

In current study, we have kept our model at the minimal level to highlight the essence of HI in the near-field limit. In principle, the description of the near-field HI by the resistance tensor is so generic that we expect the model to be broadly applicable. With moderate modifications while retaining its simplicity, our model can be generalized to bacteria with nonspherical cell bodies, other species of microswimmers, and different boundary conditions (*SI Appendix*, Figs. S3–S5). Furthermore, results of our simulations of bacterial suspensions demonstrated that our model is essential for understanding the nonequilibrium physics in active fluids: Under the same conditions, our model of HI using the resistance tensor leads to qualitatively different clustering behavior as compared to that obtained from the existing two-bead model plus a steric repulsion (*SI Appendix*, Fig. S6).

In conclusion, we have proposed a rigorous model for the near-field HI that is both physically effective and computationally efficient. Compared to the method of Stokeslets that is considered the gold standard in solving Stokes flows, our model shows equal accuracy in both the near field and the far field but drastically reduced the computational burden so that the HI of thousands of bacteria can now be evaluated by a PC in seconds. In reality, other types of interactions (e.g., steric repulsion and electrostatic interaction) exist in active fluids and may be important. Our current work points out that HI can be fully described by the resistance tensor of dissipative

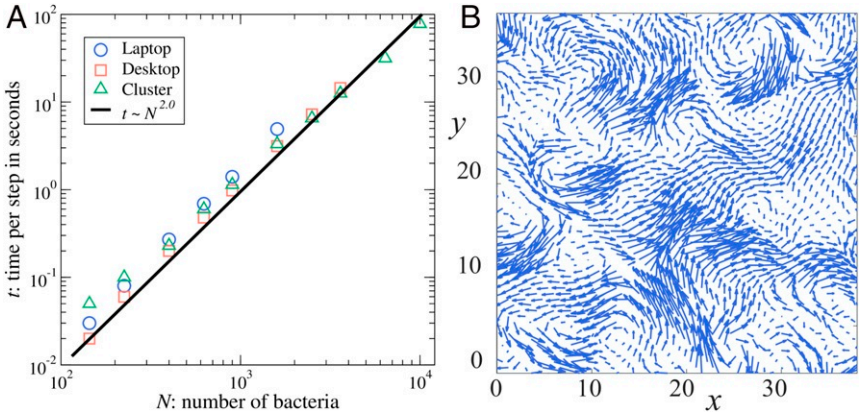

Fig. 5. Efficient simulation of bacterial suspensions. (*A*) Simulation time per step as a function of the number of bacteria. (*B*) Snapshot of the velocity field.

nature so that it is fundamentally different from interactions of conservative nature: One cannot use interactions of conservative nature in place of the HI, and vice versa. This fundamental difference justifies previous studies, where simulations of small nonequilibrium suspensions ($N \approx 100$) demonstrated that the use of a steric repulsion in place of a resistance tensor leads to qualitatively erroneous predictions regarding both system dynamical behaviors and structures (12, 13). Previous simulations of bacterial suspensions with similar tactics of using a steric repulsion to avoid proper treatment of the HI in the near-field limit are all liable to similar computational artifacts.

Data Availability. All study data are included in the article and *SI Appendix*.

ACKNOWLEDGMENTS. We thank H. Chate, L. S. Luo, and Z. G. Wang for helpful discussions. This work is supported by National Natural Science Foundation of China Grants 11974038, 11672029, U1930402, and 11904320. We also acknowledge the computational support from the Beijing Computational Science Research Center.

1. E. Lushi, H. Wioland, R. E. Goldstein, Fluid flows created by swimming bacteria drive self-organization in confined suspensions. *Proc. Natl. Acad. Sci. U.S.A.* **111**, 9733–9738 (2014).
2. A. C. H. Tsang, E. Kanso, Density shock waves in confined microswimmers. *Phys. Rev. Lett.* **116**, 048101 (2016).
3. A. Sokolov, A. Mozaffari, R. Zhang, J. J. de Pablo, A. Snezhko, Emergence of radial tree of bend stripes in active nematics. *Phys. Rev. X* **9**, 031014 (2019).
4. S. Ramaswamy., The mechanics and statistics of active matter. *Annu. Rev. Conden. Matt. Phys.* **1**, 323–345 (2010).
5. D. Saintillan, M. J. Shelley, Orientational order and instabilities in suspensions of self-locomoting rods. *Phys. Rev. Lett.* **99**, 058102 (2007).
6. S. Guo, D. Samanta, Y. Peng, X. Xu, X. Cheng, Symmetric shear banding and swarming vortices in bacterial superfluids. *Proc. Natl. Acad. Sci. U.S.A.* **115**, 7212–7217 (2018).
7. D. Saintillan, Rheology of active fluids. *Annu. Rev. Fluid Mech.* **50**, 563–592 (2018).
8. H. Xu, J. Dauparas, D. Das, E. Lauga, Y. Wu, Self-organization of swimmers drives long-range fluid transport in bacterial colonies. *Nat. Commun.* **10**, 1792 (2019).
9. A. Dehkharghani, N. Waisbord, J. Dunkel, J. S. Guasto, Bacterial scattering in microfluidic crystal flows reveals giant active Taylor–Aris dispersion. *Proc. Natl. Acad. Sci. U.S.A.* **116**, 11119–11124 (2019).
10. C. Liu, C. Zhou, W. Wang, H. P. Zhang, Bimetallic microswimmers speed up in confining channels. *Phys. Rev. Lett.* **117**, 198001 (2016).
11. S. Ketzetzi, J. de Graaf, R. P. Doherty, D. J. Kraft, Slip length dependent propulsion speed of catalytic colloidal swimmers near walls. *Phys. Rev. Lett.* **124**, 048002 (2020).
12. X. Cheng, X. Xu, S. A. Rice, A. R. Dinner, I. Cohen., Assembly of vorticity-aligned hard-sphere colloidal strings in a simple shear flow. *Proc. Natl. Acad. Sci. U.S.A.* **109**, 63–67 (2012).
13. N. Yoshinaga, T. B. Liverpool, From hydrodynamic lubrication to many-body interactions in dense suspensions of active swimmers. *Eur. Phys. J. E* **41**, 76 (2018).
14. R. Cortez, The method of regularized Stokeslets. *SIAM J. Sci. Comput.* **23**, 1204–1225 (2001).
15. K. Ishimoto, E. A. Gaffney, Boundary element methods for particles and microswimmers in a linear viscoelastic fluid. *J. Fluid Mech.* **831**, 228–251 (2017).
16. A. Poddar, A. Bandopadhyay, S. Chakraborty, Near-wall hydrodynamic slip triggers swimming state transition of micro-organisms. *J. Fluid Mech.* **9**, A11 (2020).
17. S. E. Spagnolie, E. Lauga, Hydrodynamics of self-propulsion near a boundary: Predictions and accuracy of far-field approximations. *J. Fluid Mech.* **700**, 105–147 (2012).
18. K. Drescher, J. Dunkel, L. H. Cisneros, S. Ganguly, R. E. Goldstein, Fluid dynamics and noise in bacterial cell–cell and cell–surface scattering. *Proc. Natl. Acad. Sci. U.S.A.* **108**, 10940–10945 (2011).
19. X.-L. Wu, A. Libchaber, Particle diffusion in a quasi-two-dimensional bacterial bath. *Phys. Rev. Lett.* **84**, 3017–3020 (2000).
20. Y. Peng *et al.*, Diffusion of ellipsoids in bacterial suspensions. *Phys. Rev. Lett.* **116**, 068303 (2016).
21. J. P. Hernandez-Ortiz, P. T. Underhill, M. D. Graham, Dynamics of confined suspensions of swimming particles. *J. Phys. Condens. Matter* **21**, 204107 (2009).
22. J. Dunstan, G. Miño, E. Clement, R. Soto, A two-sphere model for bacteria swimming near solid surfaces. *Phys. Fluids* **24**, 011901 (2012).
23. Y. Li, H. Zhai, S. Sanchez, D. B. Kearns, Y. Wu., Noncontact cohesive swimming of bacteria in two-dimensional liquid films. *Phys. Rev. Lett.* **119**, 018101 (2017).
24. V. Gyrya, I. S. Aranson, L. V. Berlyand, D. Karpeev, A model of hydrodynamic interaction between swimming bacteria. *Bull. Math. Biol.* **72**, 148–183 (2010).
25. J. P. Hernandez-Ortiz, C. G. Stoltz, M. D. Graham, Transport and collective dynamics in suspensions of confined swimming particles. *Phys. Rev. Lett.* **95**, 204501 (2005).
26. T. Ishikawa, M. P. Simmonds, T. J. Pedley, Hydrodynamic interaction of two swimming model micro-organisms. *J. Fluid Mech.* **568**, 119–160 (2006).
27. M. Theers, E. Westphal, K. Qi, R. G. Winkler, G. Gompper, Clustering of microswimmers: Interplay of shape and hydrodynamics. *Soft Matter* **14**, 8590–8603 (2018).
28. T. Ohmura *et al.*, Simple mechanosense and response of cilia motion reveal the intrinsic habits of ciliates. *Proc. Natl. Acad. Sci. U.S.A.* **115**, 3231–3236 (2018).
29. J. F. Brady, G. Bossis, Stokesian dynamics. *Annu. Rev. Fluid Mech.* **20**, 111–157 (1988).
30. V. A. Martinez *et al.*, Flagellated bacterial motility in polymer solutions. *Proc. Natl. Acad. Sci. U.S.A.* **111**, 17771–17776 (2014).
31. J. L. Higdon, The generation of feeding currents by flagellar motions. *J. Fluid Mech.* **94**, 305–330 (1979).
32. O. Sipos, K. Nagy, R. Di Leonardo, P. Galajda, Hydrodynamic trapping of swimming bacteria by convex walls. *Phys. Rev. Lett.* **114**, 258104 (2015).
33. D. J. Jeffrey, Y. Onishi, Calculation of the resistance and mobility functions for two unequal rigid spheres in low-Reynolds-number flow. *J. Fluid Mech.* **139**, 261–290 (1984).
34. D. Takagi, A. B. Braunschweig, J. Zhang, M. J. Shelley, Dispersion of self-propelled rods undergoing fluctuation-driven flips. *Phys. Rev. Lett.* **110**, 038301 (Jan 2013).
35. S. E. Spagnolie, G. R. Moreno-Flores, D. Bartolo, E. Lauga, Geometric capture and escape of a microswimmer colliding with an obstacle. *Soft Matter* **11**, 3396–3411 (2015).
36. S. Kim, S. J. Karrila, *Microhydrodynamics: Principles and Selected Applications* (Dover Publication, New York, NY, 2005).
37. A. Zottl, H. Stark, Hydrodynamics determines collective motion and phase behavior of active colloids in quasi-two-dimensional confinement. *Phys. Rev. Lett.* **112**, 118101 (2014).
38. M. Theers, E. Westphal, G. Gompper, R. G. Winkler, Modeling a spheroidal microswimmer and cooperative swimming in a narrow slit. *Soft Matter* **12**, 7372–7385 (2016).
39. M. Kuron, P. Stärk, C. Burkard, J. De Graaf, C. Holm, A lattice Boltzmann model for squirmers. *J. Chem. Phys.* **150**, 144110 (2019).
40. J. J. Molina, Y. Nakayama, R. Yamamoto, Hydrodynamic interactions of self-propelled swimmers. *Soft Matter* **9**, 4923–4936 (2013).